Journal of
Engineering Sciences
Faculty of Engineering
Assiut University
JES
مجلة
العلوم الهندسية
كلية الهندسة
جامعة أسيوط
journal homepage: http://jesaun.journals.ekb.eg

Response of Single Plane Reinforced Concrete Cable-Stayed Bridge with Prestressed Deck under Blast Load

Received 7 March 2024; Revised 28 May 2024; Accepted 28 May 2024

Mohamed N. Elansary[1]
Eehab Khali l[2]
Mohamad A. Hasan [3]

Keywords
Cable-stayed bridge,
Structural Response,
Prestressed Concrete,
Blast load.

Abstract: Studies on cable-stayed bridges exposed to blast loads encounter significant challenges arising from the complex interaction among different structural elements. Despite extensive investigation into how buildings respond to explosive loads, there is limited literature on the dynamic response of prestressed concrete bridge decks to blast loads. Single plane cable stayed bridges are very sensitive to cable loss or degradation. This study investigates the response of a prestressed concrete cable-stayed bridge with a single plane under blast loads, utilizing a comprehensive Finite Element (FE) model that incorporates nonlinear effects. The investigation considers blast weights of 230 kg, 680 kg, and 2270 kg of TNT. The analysis reveals that even small explosions cause damage to the deck, with more significant effects observed under higher blast loads, resulting in a damaged region measuring 12 m x 10 m with a 2270 kg TNT weight. Forces in cables near the detonation point increase by 19% during a 2270 kg TNT explosion. Notable changes are observed in pylon moments under different explosion charges. Maximum Bending Moment (BM) values are observed at the base under dead loads, while BMs at mid-height increase under various blast weights, with no discernible change at the base. This study provides valuable insights for designers, emphasizing the importance of incorporating explosion-resistant design principles into cable-stayed bridges.

1. Introduction

In the last six decades, more than 550 terrorist attacks have targeted bridges and related infrastructure [1]. Cable-stayed bridges, being vital public infrastructure, require protection

[1] Teaching assistant, Construction and Building. Engineering Department, College of Engineering and Technology, Arab Academy for Science, Technology & Maritime Transport, Egypt. moh.nasr111@aast.edu
[2] Professor, Construction research institute, National water research centre, Egypt. DR.eehab@gmail.com
[3] Assoc. professor, Construction and Building. Engineering Department, College of Engineering and Technology, Arab Academy for Science, Technology & Maritime Transport, Egypt. m.shakour@aast.edu

https://doi.org/10.21608/JESAUN.2024.275263.1318

to ensure operational safety and prompt response during natural disasters or intentional acts of destruction, such as explosions resulting from vehicle collisions or terrorist attacks [2]. Protecting cable-stayed bridges against progressive failure due to explosive threats was investigated [3]. Recent research highlights the importance of incorporating explosions into structural design, focusing on how structures respond to explosive shock waves. This shift provides guidance on mitigating explosion damage, in contrast to earlier studies that often concentrated on individual structural components [4]. In 2007 Trélat [5] used numerical simulations to analyze how a structure responds to a strong explosion, highlighting significant damage and factors like explosion location and charge size. Lellep [6] studied rigid-plastic beams under impulsive loading, revealing plastic deformation, buckling, and failure, confirming the need to consider impulsive loading in design. In 2021 [7], experiments on a T-beam bridge exposed to blast loading demonstrated concrete spalling, rebar rupture, and beam cracking. This underscores the crucial need to consider blast loading in T-beam bridge design and offers ways to enhance their blast resistance. Studies of reinforced concrete beams under impact and blast loads unveiled incidents such as flexural cracking, spalling, and reinforcement yielding, particularly at elevated loading rates [8]. Numerical simulations showed blast-induced damage in concrete bridge columns, including spalling, rebar fracture, and buckling. Blast intensity, distance, and column shape affected the damage, highlighting the need to consider blast loading in column design [9].

In 2023, Anas [10] use FEM to examine how support conditions (simply vs. three-edge) and material (standard vs. UHPC) affect square RC slabs under low-velocity impacts (displacement, stress/strain, cracks, failure). This informs design for such impacts. An experimental and numerical study reviews existing research on blast response of RC slabs [11]. It analyzes findings, challenges, and future directions, emphasizing blast resistance for security/defense structures.

The significance of blast analysis in cable-stayed bridge research is growing, and several studies are now evaluating the performance of reinforced concrete bridges subjected to blast loads. Numerical analysis was employed to study cable-stayed bridge's response to blasts, proving that blast load magnitude and distance from the explosion point impact the bridge's dynamics [12]. Retrofitting for blast resistance was examined where it enhances strength and reduce damage [13]. [14], [15] present two papers in a series on numerical simulation of a cable-stayed bridge's blast load response. The first paper describes the model and blast load calculations. The second paper predicts bridge damage and uses FRP to increase blast resistance. In [16] Tetougueni's study utilized numerical simulations and experiments on a scaled-down bridge model to explore blast factors like distance, weight, and structure. The research focused on analyzing bridge deck deformation and stress distribution under varying blast magnitudes and distances. Also [17] used numerical analysis and experiments to study how different blast magnitudes and distances affect pylon's response to blast loads. Zhu's recent study [18] assessed composite bridge slabs' strength to contact explosions. Common damage patterns like concrete spalling, steel plate deformation, and slab detachment were observed in all three slabs. The extent of damage varied based on the concrete-slab interface type and steel plate thickness during contact explosions. In 2021, Hassan [19] concluded that

post-tensioned cables and pretension strands remained intact in most blast scenarios, indicating their resilience to explosive forces. The deck experienced damage even in small explosions.

Fig. 1 shows the idealized pressure profile over time for a free air blast wave. In this context, the duration for the pressure to reach its maximum value is negligible and is commonly treated as zero for design purposes. The peak overpressure, labeled as P_{so}, is reached at this juncture. Following this, the pressure decreases exponentially until it returns to ambient levels at t_A+t_o, where to signify the positive phase duration [20]. The study focused on non-contact, unconfined external explosions, shown in **Fig. 2**. These explosions can be classified into three fundamental types determined by the relative positioning of the explosive source and the protected structure. The categorization hinges on two crucial factors: the height (H_c) above the ground where the charge (W) is detonated and the horizontal distance (R_G) between the explosive's projection on the ground and the structure [21].

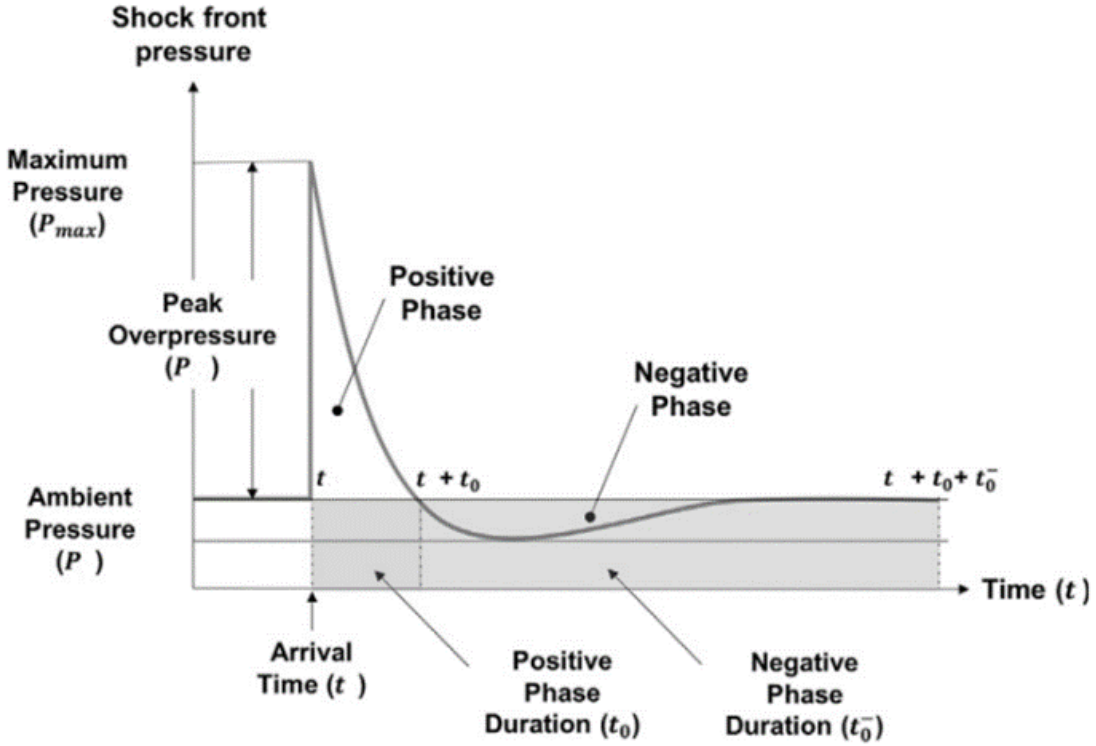

Fig. 1: Pressure-time profile of an ideal blast wave.

In the field of explosion analysis, various relationships and methodologies have been developed to calculate the incident pressure at distances from the detonation source. Among these approaches, there is a widespread agreement on employing the **Z** scale value in combination with different constants and equation formulas. These established frameworks have gained considerable recognition for their efficacy in offering accurate estimations of incident pressure. Several mathematical formulas exist for computing pressure values. ***Kinney*** introduced a specialized formulation designed for analyzing chemical explosions [22]. ***Brode's*** equations [23], depend on the magnitude of the explosion, while ***Newmark*** [24] devised a widely used alternative formulation for calculating peak overpressure values

resulting from ground surface blasts. ***Mills*** has made a significant contribution to this field by introducing a simplified expression for peak overpressure [25]. ***Kingery-Bulmash*** introduced pressure equations, compared various formulas, and highlighted deviations in ***Brode, Newmark, and Mills*** equations at small distances, attributing it to their focus on nuclear explosions. They also offered practical analytical relationships expressed as polynomial functions of the logarithm of the scaled distance, suitable for programming. It has been adopted and widely used in the field of engineering [26].

Extensive studies have examined the response of buildings, steel bridges, and concrete cable stayed bridges with two plane system designs to blast loads. However, a critical knowledge gap exists regarding the dynamic behavior of single-plane cable-stayed bridges featuring prestressed concrete decks when subjected to explosions. This study addresses this gap with a focus on the straining actions experienced by this specific bridge configuration under blast scenarios. The findings aim to contribute significantly to the field by providing valuable insights for engineers to improve the blast resistance of cable-stayed bridges.

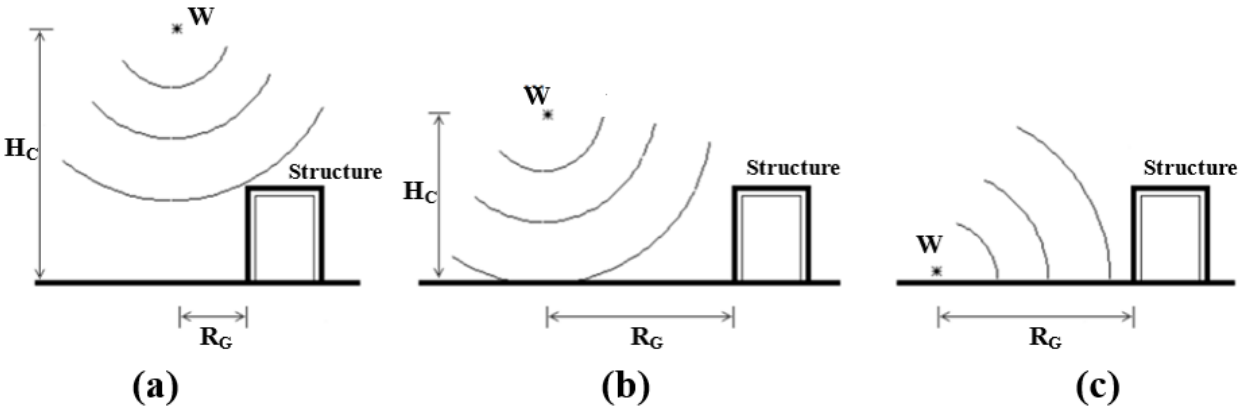

Fig. 2: Types of external explosion and blast loading;
(a) Free-air bursts, (b) Air bursts, and (c) Surface bursts [27].

2. Methods and tools

The research commenced by creating a detailed bridge model using SAP2000 software. Loads and cable forces were assigned, with adjustments made to cable forces until zero deflection along the bridge deck was achieved. Authors then thoroughly validated the model's accuracy and reliability before subjecting the bridge to blast loads. The methodology adopted in this study is outlined in the flow chart depicted in **Fig. 3**.

2.1. Finite Element (FE) Model

Cable-stayed bridges, featuring a single cable plane supporting a prestressed concrete box girder, present a compelling design. The ***Aswan Bridge*** exemplifies these characteristics, with a 500 m long main cable-stayed bridge. The cast-in-place segmental deck is suspended from fourteen pairs of stay cables arranged in a central layer and supported by two Prestressed

Concrete (PC) pylons, as illustrated in **Fig. 4**. Cables Cross-sectional areas differ as shown in **Table 1**, with parallel strands of 1860 MPa ultimate tensile strength.

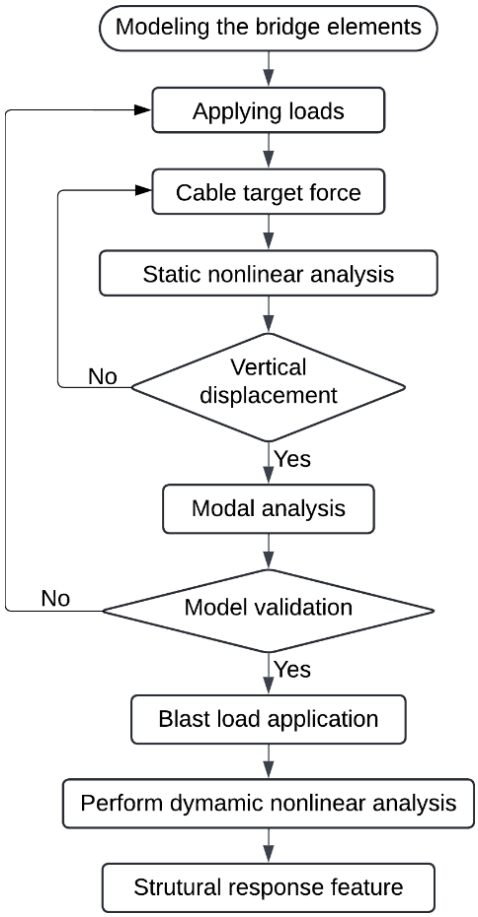

Fig. 3: Flow Chart Showing Research Methodology.

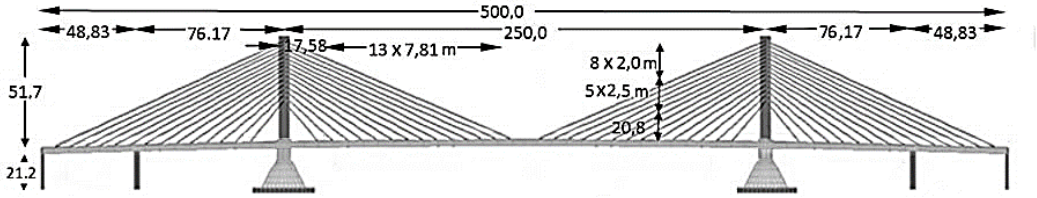

Fig. 4: Aswan Cable Stayed Bridge.

Table 1: Cross sectional area of cables.

Label		**Area (mm^2)**	**Label**		**Area (mm^2)**
Main span	**Side span**		**Main span**	**Side span**	
MC01	SC01	16300	MC08	SC08	13600
MC02	SC02	16300	MC09	SC09	13200
MC03	SC03	15900	MC10	SC10	12300
MC04	SC04	15500	MC11	SC11	10900
MC05	SC05	15300	MC12	SC12	9900
MC06	SC06	15000	MC13	SC13	9900
MC07	SC07	14700	MC14	SC14	9900

To consider the nonlinearity of the cables and incorporate the impact of sagging, the Ernst coefficient was employed. The actual stress was considered in the sequential load cases for modeling, as depicted in **Eq. (1)**.

$$E_{eff} = E_0 \frac{1}{1+\frac{\gamma^2 L_h^2 E_0}{12\sigma^3}} \qquad \textbf{Eq. (1)}$$

Where:

E_{eff}	=	The effective elastic modulus taking into consideration sagging effect (N/mm^2)
E_0	=	The elastic modulus of cable material (N/mm^2)
γ	=	The specific weight of cable material (N/mm^3)
σ	=	The axial stress in cable (N/mm^2)
L_h	=	The projected length of cable in plan (mm)

The bridge features a single-cell trapezoidal section, measuring 3.3 m in height and 24.3 m in width, with a slim 220 mm top slab as illustrated in **Fig. 5.a**. To accurately represent the complete behaviour of the deck, a plate-membrane (shell) element model, incorporating longitudinal and transversal prestressing tendons in the top slab, was utilized. Additionally, 52.0-meter-height pylons made of prestressed concrete are depicted in **Fig. 5.b**. This model is designed to replicate the stiffness characteristics of a genuine box-girder, detailed in **Table 2** [28]. Plastic hinges (PH) were integrated into both cables and the top beam, as shown in **Fig. 5.c**, to accommodate plastic deformations resulting from additional stresses due to blast loads.

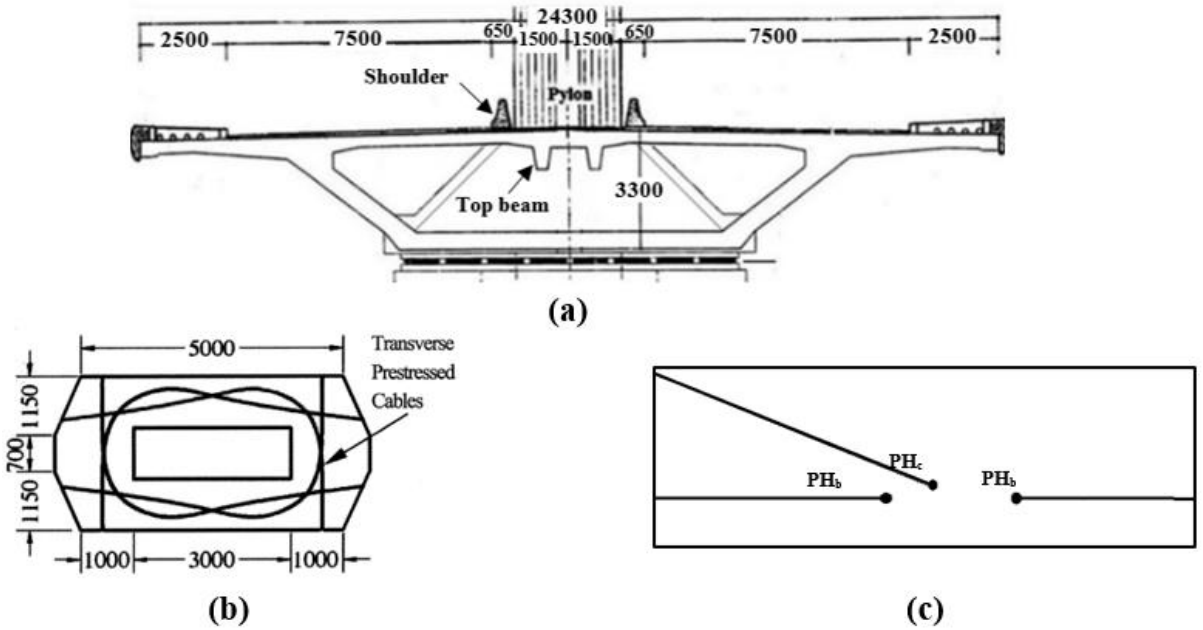

Fig. 5: The section of bridge main elements;
(a) Pylon section (Unit: mm), (b) Deck section (Unit: mm), and (c) Location of plastic hinges.

Material models were created for steel (FY = 360 MPa, f_{su} = 520 MPa, E_s = 210,000 MPa) and concrete ($f_{c'}$ = 46 MPa) considering confinement and considered the damping ratio based on the principles of Rayleigh damping to accurately simulate the dynamic response of the structure. A sectional analysis evaluated the non-linear relation between moment and curvature (flexibility) based on member dimensions and reinforcement. Established models by Park (1982) [29] and Mander (1988), [30] were used to define the stress-strain behaviour for steel and confined concrete, respectively (**Fig. 6**). The software analysis employed the Takeda Hysteresis Model to simulate the nonlinear dynamic properties of materials, which proved less effective in our study, focused on a single blast event. Since our analysis does not involve repeated loading cycles. Additionally, prestressed concrete exhibits a unique characteristic where prestressing elevates the grade of the concrete, resulting in a dynamic response closely resembling static behaviour.

Table 2: Section properties.

Element	Cross-sectional area A (m^2)	Moment of inertia about x-axis I_x (m^4)	Moment of inertia about y-axis I_y (m^4)	Torsion constant J (m^4)
Deck section	14.560	22.407	530.730	54.000
Pylon	14.100	44.048	12.575	25.959

The traffic loads on roadway bridges, comprised both concentrated and distributed loads in accordance with the specifications of the first case of loading in the Egyptian code 201. Target force loading involves a nonlinear-static application where the desired cable tension is defined. Iterative deformation load application is performed until the target tension is reached. A scale factor is applied to the load pattern containing the target-force load to adjust the target force. To apply target forces, 100 iterations per stage are required, with a relative convergence tolerance of 0.002. A mesh convergence study has been conducted to assess result sensitivity to mesh density. The mesh size varied throughout the model, ranging from a fine mesh of 0.25 m in blast load areas to a coarser mesh of 1 m in less critical locations. This approach balances accuracy in key areas with computational efficiency. Following that, the verification and validation process for model accuracy to be emphasized. Modal analysis was conducted to identify mode shapes in the FE model, and validation was achieved by comparing these mode shapes with selected mode shapes from previous experimental study [31] shown in **Table 3.** The comparison involved a detailed analysis of numerical and experimentally identified modes of the deck, with differences in frequencies found to be less than 5%. Then to verify the complex response under blast loads, a practical approach involved simulating a 230 kg TNT scenario using two software tools: SAP2000 and ANSYS WORKBENCH. ANSYS, known for its reliability in blast simulations [32], [33], allowed comparison of stresses and damage extent on the top slab deck. The close convergence between the software results (**Fig. 7**) and the stress level comparison in **Table 4** verified the FE model and highlighted the importance of accurate stress prediction for bridge integrity.

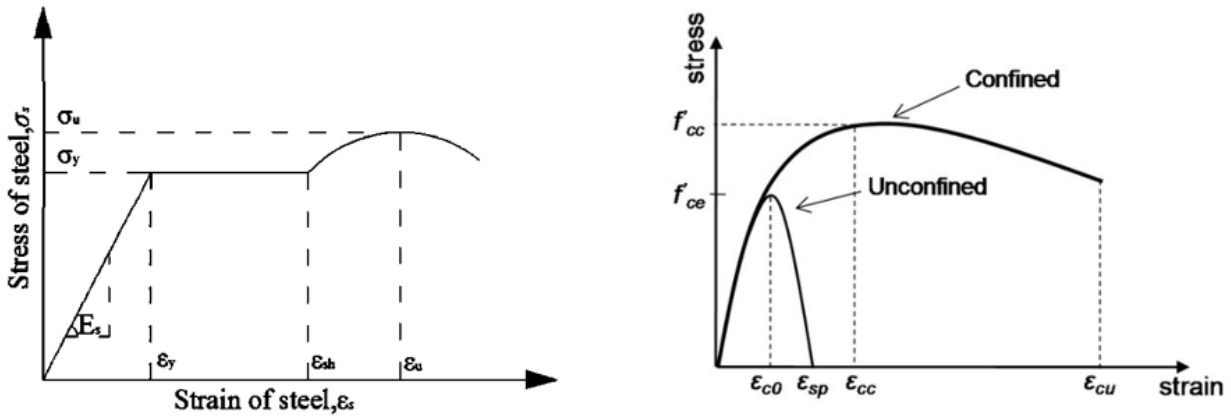

Fig. 6: Material characterization for hinge properties.
Steel material, and (b) Concrete material.

Table 3: Numerical mode shapes and frequencies for deck.

Mode Order	Mode Type	Front View/3D View	Numerical Freq. (Hz)	Experimental Freq.	% Difference
1	Bending		0.490	0.486	+0.82
2	Bending		0.834	0.842	-0.96
3	Bending		1.360	1.42	-4.4

Table 4: Comparison of results between the two software programs.

Compression aspect		CSI SAP 2000	ANSYS WORKBECH	% Difference
Damage limits	L (m)	1.10	1.15	4.35
	W (m)	0.67	0.70	4.48
Max. stress (N/mm^2)		53.20	52.66	1.01

2.2. Blast parameter calculation

Understanding various blast scenarios and potential explosion sizes is crucial for assessing structural vulnerability and developing effective blast mitigation strategies. The exact explosion conditions on a bridge can be unpredictable, stemming from sources like terrorist acts or accidents involving fuel tankers. While the quantity of explosives and detonation energy may remain unknown, the means of transporting explosive materials on the bridge

(e.g., car, van, or truck) and their capacities can be estimated [34]. According to FEMA [35] recommendations, and assumptions regarding different-sized fuel tanker explosions is shown in **Table 5**.

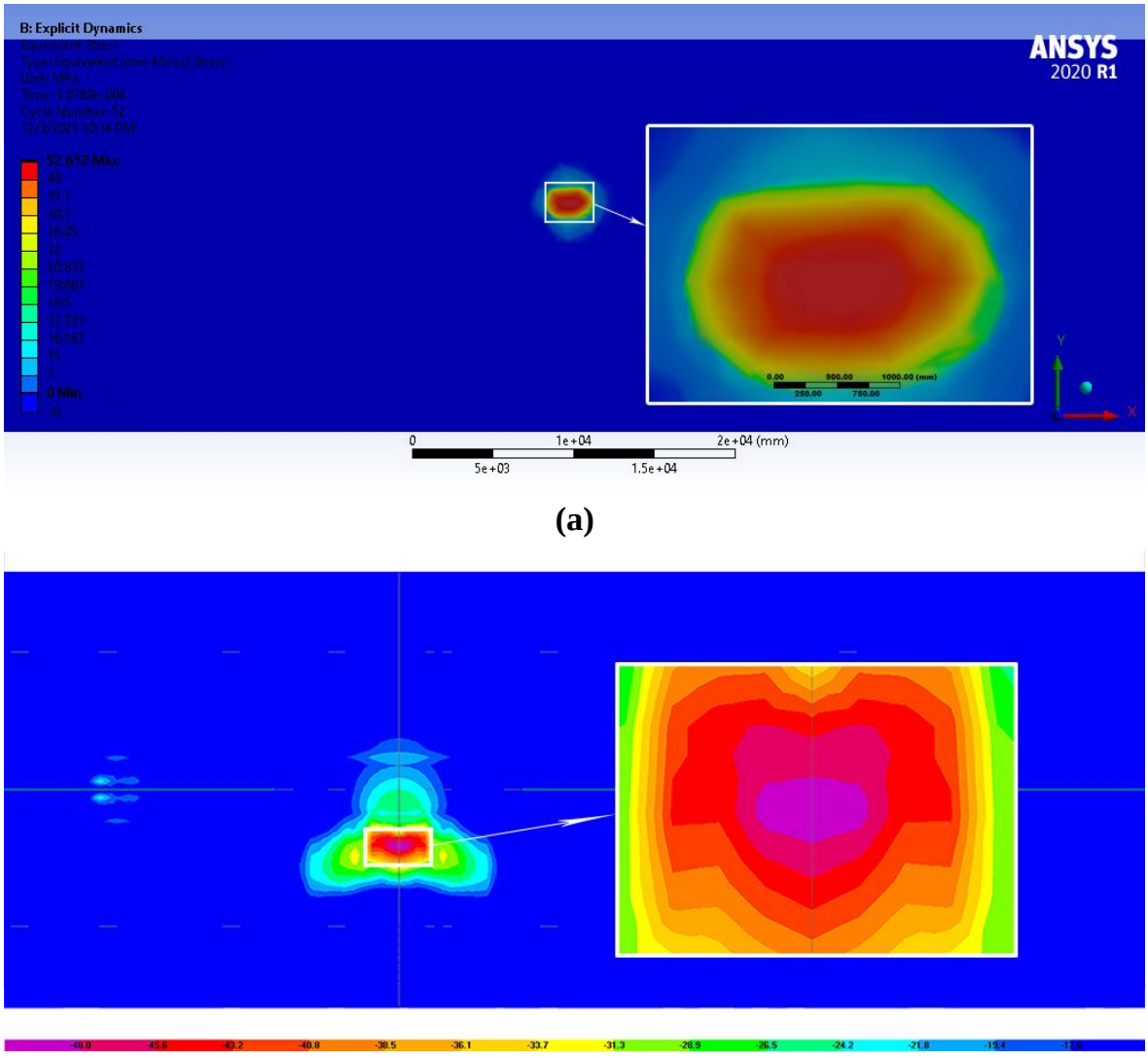

(a)

(b)

Fig. 7: Stresses and damage limits due to the blast load on the top slab.
(a) ANSYS Workbench stress contour, and (b) SAP2000 stress contour.

Table 5: Maximum permitted load capacity for each mode of transportation.

Carrier	**Explosive weight of TNT (kg)**
Suitcase	10
Medium-sized car	200
Large-sized car	300
Pick-up truck	1400
Van	3000

The Kingery-Bulmash method was employed to calculate the pressure-time history, including its peak magnitude, total impulse, and durations (**Fig. 8**) for the free-air burst loading type.

While the method captures the positive pressure phase crucial for design, it's important to acknowledge that design practices often disregard the negative pressure phase due to its typically longer duration and lower peak pressure compared to the positive phase [36]. Understanding and analyzing blast loads can be challenging. To simplify calculations and analysis, these blast loads are represented as an equivalent time history load. The study examines a critical scenario involving an explosion at the mid-span of a cable-stayed bridge. Three different TNT weights (230 kg, 680 kg, and 2270 kg) were examined to assess the bridge's response.

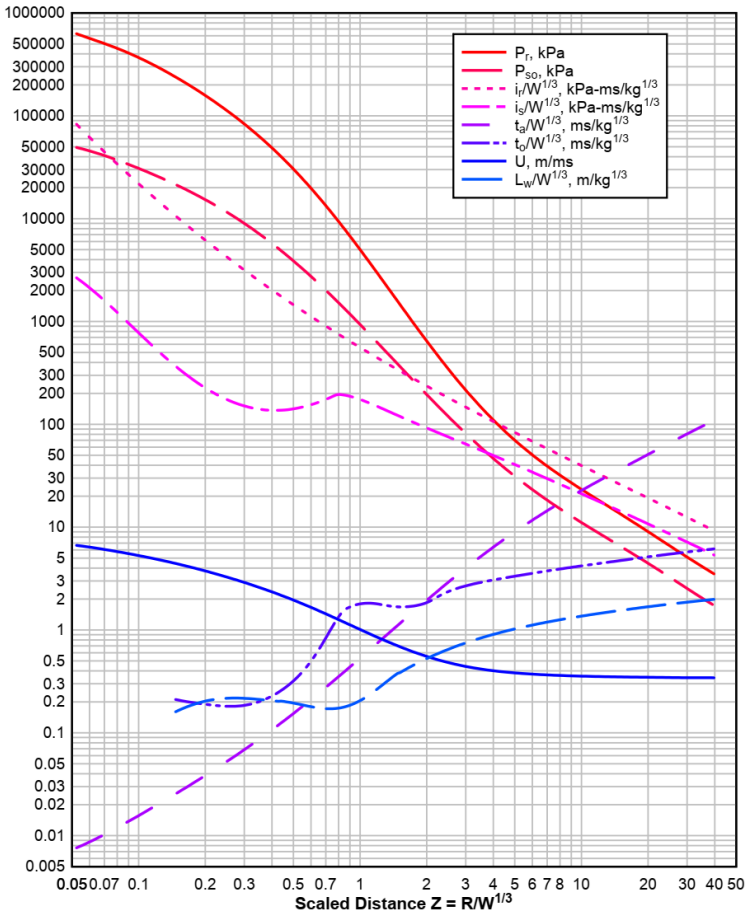

Fig. 8: Parameters of the positive phase of shock spherical waves from TNT charges in free-air bursts [27].

The considered scenario is the presence of a vehicle like a car, or a regular truck commonly used for transporting explosives driving in the traffic lane near the shoulder. Three different blast loads are explored. The explosion point is assumed to be on the truck bed, positioned 1m above the ground. The analysis focuses on distances ranging from 1m to a maximum of 7.62m as shown in **Fig. 9**. These distances are used to calculate the corresponding blast loads applied to the bridge during the analysis. Blast pressure weakens with distance from the explosion, following a spherical distribution. Pressure perpendicular to the surface has the most impact, while pressure at shallow angles dissipates through reflection. It is assumed that

when a streak of pressure strikes the surface at an angle of approximately 30 degrees or less, it imparts less force and dissipates through reflection.

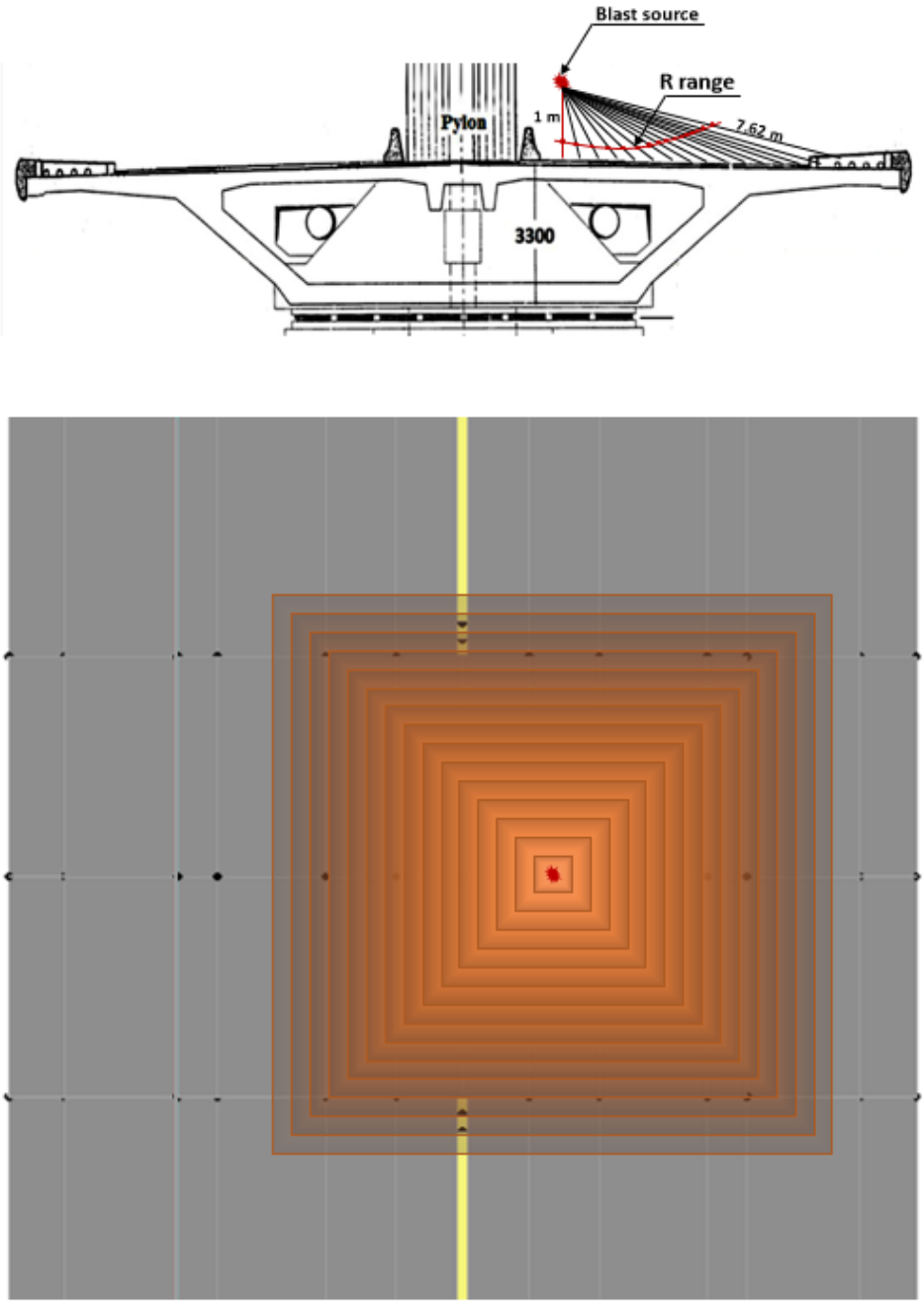

Fig. 9: The orientation and effective range of blast scenario.

To streamline the blast distribution method, it is further assumed that the blast pressure beyond the region projected at a 30-degree angle has negligible impact on the structure [37]. **Eq. (2)**, which inversely relates blast pressure to scaled distance ***Z*** was employed [27].

$$Z = {R}/{W^{(1/3)}} \qquad \textbf{Eq. (2)}$$

Where:

R = The distance from detonation point to the point of interest (m)
W = The weight of TNT explosion (kg).

To apply the blast loads generated by selected explosion weight, different time history curves were developed to cover the effective range, guided by ***Kingery-Bulmash*** curves. Details of the resulting loads are given in **Table 6**. **Fig. 10** shows Pressure-time histories Curves for a load of 230 kg of TNT.

Table 6: Blast load parameters.

	Standoff distance (R) (m)	**1.35**	**1.7**	**2.18**	**2.7**	**3.25**	**3.82**	**4.4**	**4.98**	**5.56**	**6.16**	**7.62**
230 kg TNT	Z (m/kg$^{1/3}$)	0.22	0.28	0.36	0.44	0.53	0.62	0.72	0.92	0.91	1.01	1.24
	t_A (msec)	0.29	0.37	0.55	0.92	1.13	1.47	1.84	2.39	2.94	3.43	4.91
	P_{so} (t/m^2)	1300	900	650	460	320	250	180	150	110	90	51
	i_s (t/m^2.msec)	122.5	104.2	91.90	85.78	98.03	110.3	116.4	122.5	119.5	113.3	98
	t_d (msec)	0.48	0.60	0.83	1.29	1.75	2.35	3.13	4.02	5.11	5.95	8.75
680 kg TNT	Z (m/kg$^{1/3}$)	0.15	0.19	0.25	0.31	0.37	0.43	0.50	0.57	0.63	0.70	0.87
	t_A (msec)	0.25	0.35	0.47	0.62	0.79	1.14	1.49	1.76	2.29	2.55	3.70
	P_{so} (t/m^2)	2050	1800	1200	900	650	475	400	320	280	200	140
	i_s (t/m^2.msec)	272.6	193.5	158.3	131.9	123.1	123.1	131.9	140.7	149.5	158.3	175.9
	t_d (msec)	0.51	0.57	0.74	0.91	1.17	1.66	2.15	2.64	3.35	4.13	6.21
2270 kg TNT	Z (m/kg$^{1/3}$)	0.10	0.13	0.17	0.21	0.25	0.29	0.34	0.38	0.42	0.47	0.58
	t_A (msec)	0.24	0.26	0.38	0.53	0.71	0.84	1.05	1.22	1.58	1.88	2.37
	P_{so} (t/m^2)	3005	2800	1950	1720	1150	930	740	650	520	410	290
	i_s (t/m^2.msec)	985.7	657.1	400.8	302.7	236.6	216.8	203.7	197.1	197.1	200.4	210.3
	t_d (msec)	0.89	0.73	0.79	0.88	1.12	1.31	1.60	1.83	2.34	2.86	3.82

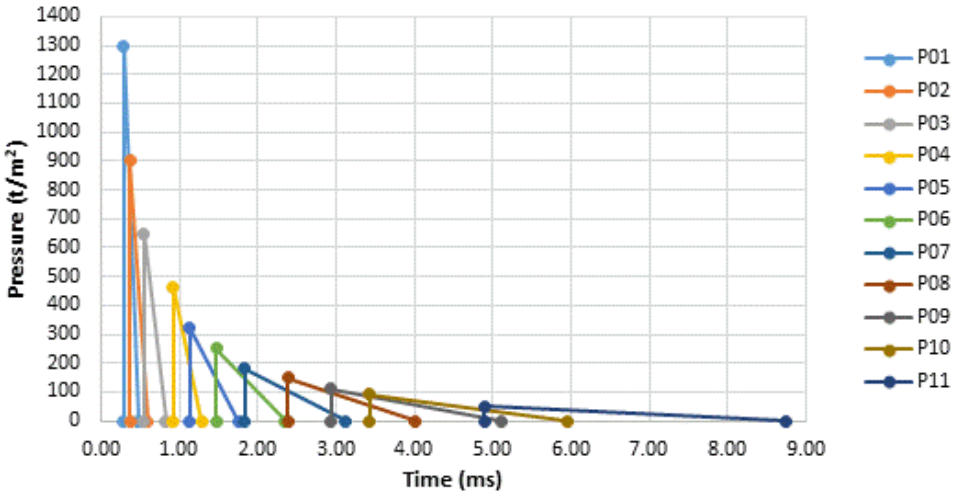

Fig. 10: Blast load time histories for 230 kg TNT.

3. Results and discussion

This study delves comprehensively into the outcomes derived from an intricate nonlinear dynamic analysis conducted on a simulated cable-stayed bridge, which was subjected to blast loads. The principal objective of this investigation was to thoroughly scrutinize and gain insights into the behaviour of three pivotal structural elements: the cables, deck, and pylon, under the influence of blast-induced loading conditions. By meticulously examining the responses of these key components, this study aims to contribute significant findings that offer deeper understanding and appreciation of the overall structural integrity and resilience inherent in cable-stayed bridge designs.

3.1. Cables force analysis

Examining the main span cables in **Fig. 11.a** reveals distinct force alterations in the first seven cables. The eighth and ninth cables converge in forces, while the remaining cables show no significant change. For the first weight (230 kg TNT), the cable nearest to the detonation point (MC01) registers a force of 10030 kN. The highest recorded value is in the second cable (MC02) at 10269 KN, representing a notable 9% increase compared to the force under main loads. The second weight (680 kg TNT) follows a similar pattern, with the nearest cable reaching 10282 KN, and the highest force observed in the second cable at 10547 KN, signifying an 11.7% increase. The peak force recorded in the cables is in the second cable at 11221 KN, reflecting a 19% increase. The most substantial percentage increase, noted in the cable nearest to the detonation point, is 19.5% for the third weight (2270 kg TNT).

For the side span cables in **Fig. 11.b**, there is a noticeable shift in force, except for the last four cables (SC11-SC14), where the change is slight. Despite the blasting load primarily affecting the main span, a noticeable impact is observed on the side span cables. This underscores the complexity of a highly indeterminate structural system, leading to intricate force interplay and distribution within the cables. Regarding the first weight, the highest force on the side cable (SC01) reaches 10237 KN, indicating a 4% increase compared to the force generated under main loads. The second weight shows a similar trend, with a maximum force of 10347 KN in the cable, resulting in a 5.2% increase. The most significant recorded increase in cables occurs with the third weight, reaching 10457 KN, reflecting a 6.4% increase.

Fig. 12 delves into cable capacity and the effects of blasting loads, focusing on the ratio of cable force for main cables (**Fig. 12.a**). Under main loads, these cables endure loading between 37.8% and 43.5% of their maximum capacity, ensuring safety across diverse scenarios. The design's ample safety factor enables cables to withstand increased blast loads. Under the first blast weight, the percentage fluctuates between 38.5% and 44.2%, attributed to increased cables near the detonation point and a slight decrease in distant ones. The second blast weight follows a similar trend, with percentages ranging from 38.5% to 45.1%. The third weight exhibits the highest increase, ranging from 38.5% to 46.5%. **Fig. 12.b** examines side cables, revealing load percentages from 39.4% to 46.8% under main loads. The consistent pattern shows a slight rise in all cables, with the first weight ranging from 40.9% to 47.5%,

the second from 41.3% to 47.6%, and the third, as expected, reaching the highest increase, from 41.6% to 48%.

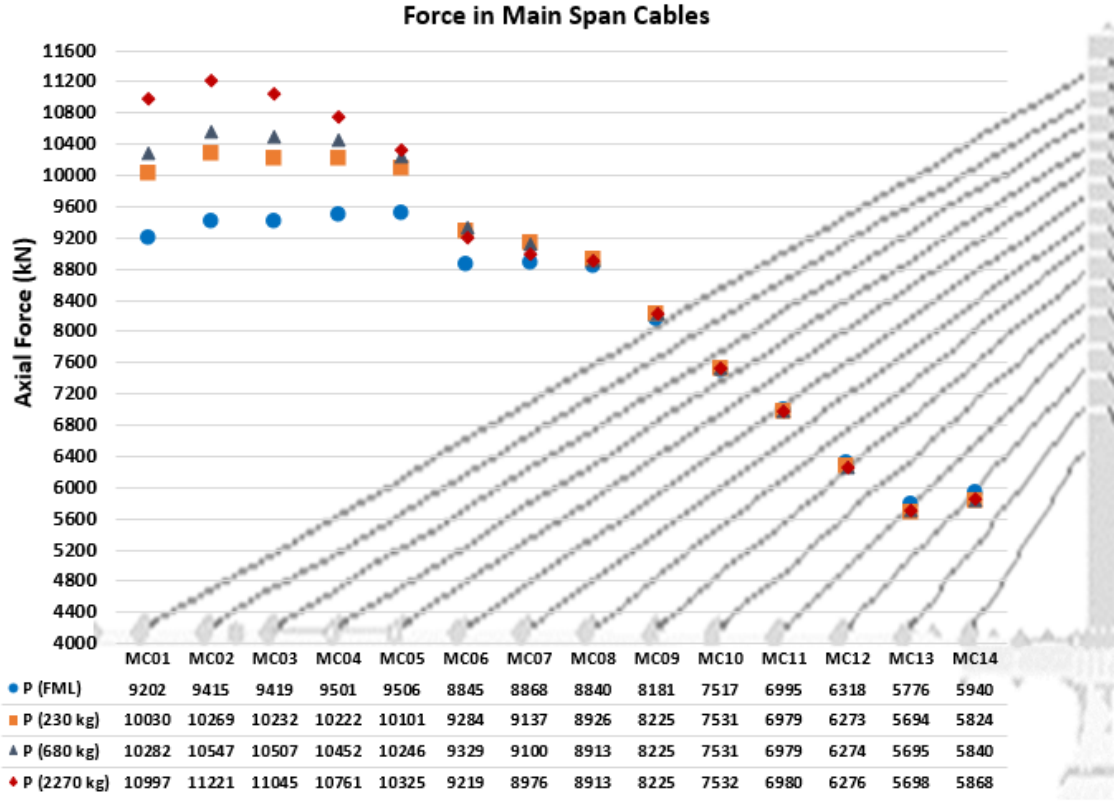

	MC01	MC02	MC03	MC04	MC05	MC06	MC07	MC08	MC09	MC10	MC11	MC12	MC13	MC14
P (FML)	9202	9415	9419	9501	9506	8845	8868	8840	8181	7517	6995	6318	5776	5940
P (230 kg)	10030	10269	10232	10222	10101	9284	9137	8926	8225	7531	6979	6273	5694	5824
P (680 kg)	10282	10547	10507	10452	10246	9329	9100	8913	8225	7531	6979	6274	5695	5840
P (2270 kg)	10997	11221	11045	10761	10325	9219	8976	8913	8225	7532	6980	6276	5698	5868

(a)

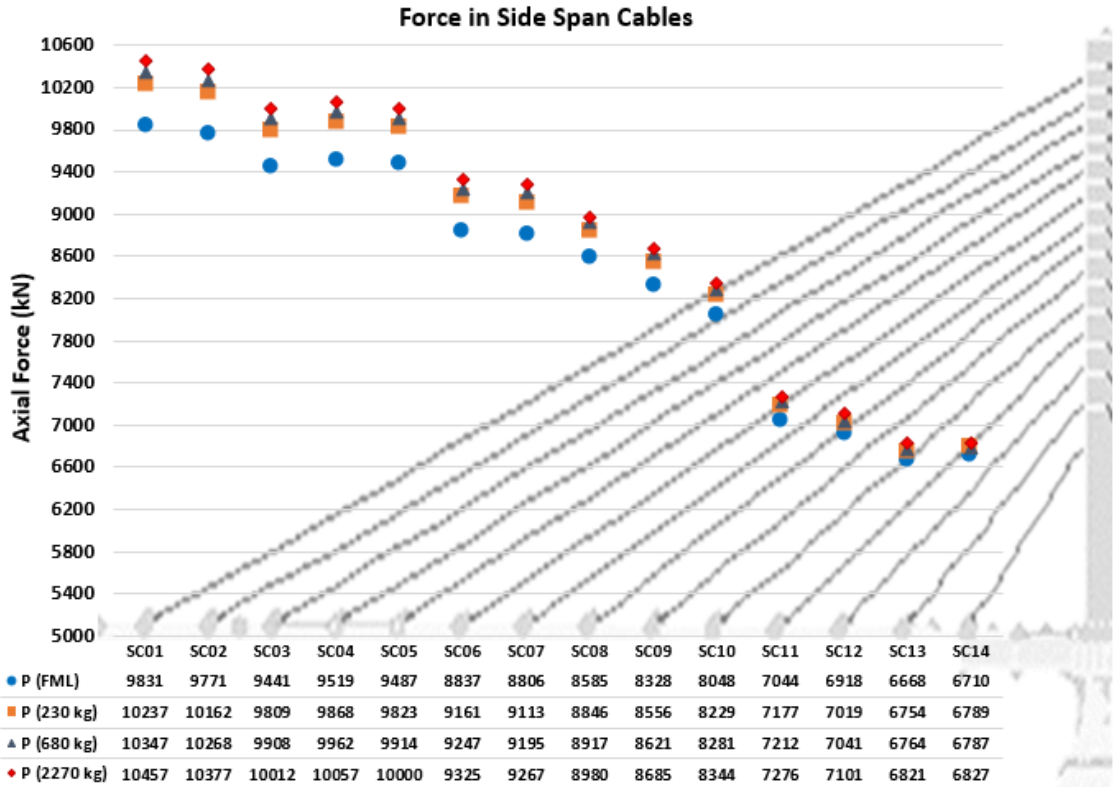

	SC01	SC02	SC03	SC04	SC05	SC06	SC07	SC08	SC09	SC10	SC11	SC12	SC13	SC14
P (FML)	9831	9771	9441	9519	9487	8837	8806	8585	8328	8048	7044	6918	6668	6710
P (230 kg)	10237	10162	9809	9868	9823	9161	9113	8846	8556	8229	7177	7019	6754	6789
P (680 kg)	10347	10268	9908	9962	9914	9247	9195	8917	8621	8281	7212	7041	6764	6787
P (2270 kg)	10457	10377	10012	10057	10000	9325	9267	8980	8685	8344	7276	7101	6821	6827

(b)

Fig. 11: Axial force for cables, (Unit: KN); (a) Main span cables, (b) Side span cables.

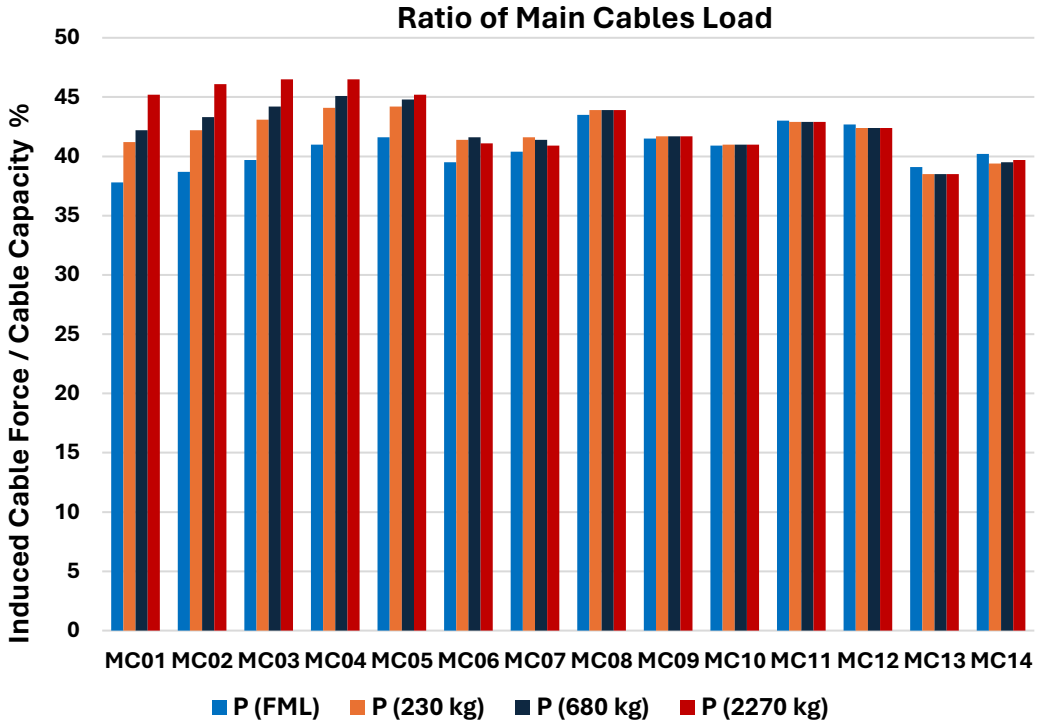

(a)

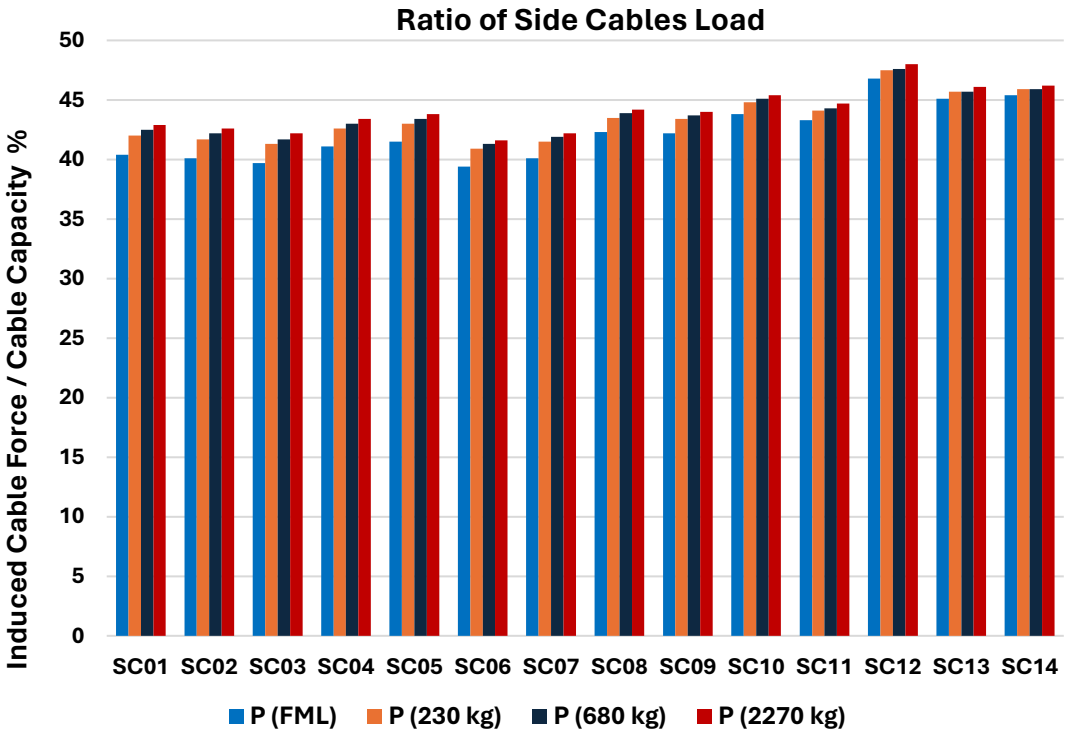

(b)

Fig. 12: Ratio of Cables force; (a) Main Span Cables, (b) Side Span Cables.

3.2. Deck response analysis.

This section focuses on the comprehensive examination and analysis of stresses and deflections on the top slab of the deck. The top slab is particularly crucial as it represents the component nearest to the exposure of blasting loads. **Fig. 13** illustrates the deflection along the top slab of Deck Bridge in the first scenario. The maximum deflection value, influenced by the main loads, reached 274 mm. Subsequently, the deflection increased with the impact of the first, second, and third explosion weights, reaching 401 mm, 444 mm, and 528 mm, respectively.

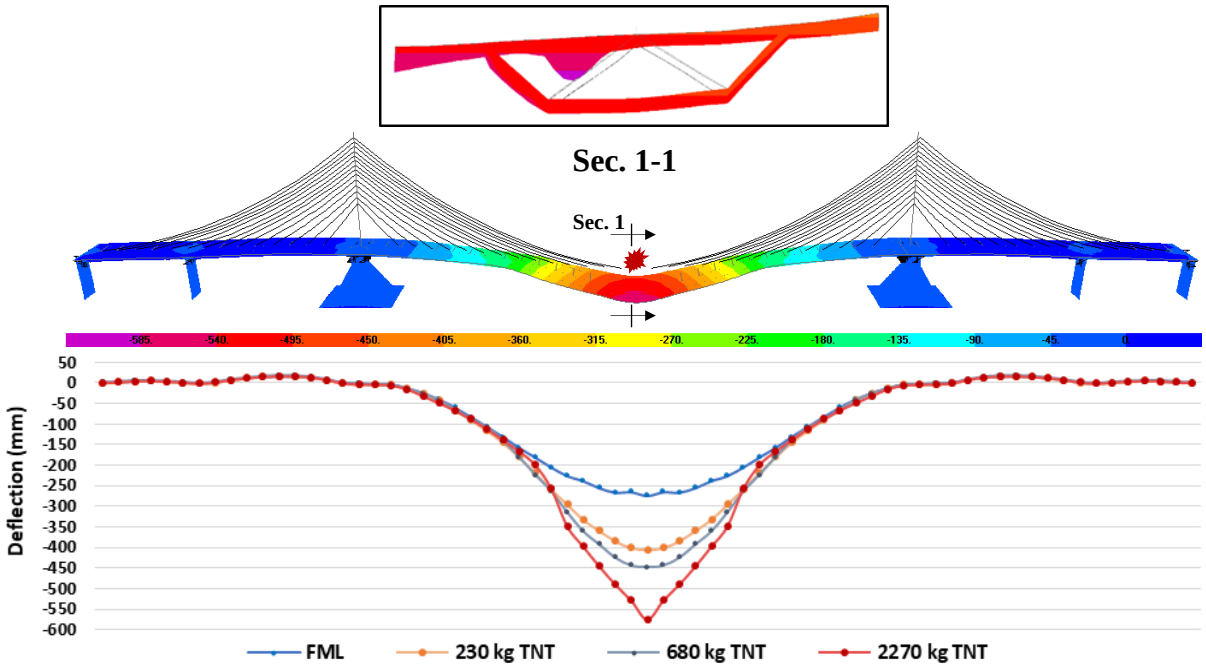

Fig. 13: Top slab deflection along the deck, (Unit: mm).

The blast loads on the bridge deck induce significant pressure on the top slab, causing large deflections expected to surpass the allowable compressive strength level of [48 N/mm^2], especially near the detonation point. **Fig. 14** displays stress contours on the top slab, highlighting regions with concentrated elevated stresses and areas exceeding the allowable stress capacity. In **Fig. 14.a**, the first explosive weight caused minor damage in a 1.15 m x 0.75 m area of the top slab. The connection zone between the cable and the deck, reinforced with the top beam, remained within its capacity, indicating effective shock resistance with minimal losses. For the second explosive weight (**Fig. 14.b**), increased pressure on the top slab led to larger losses, damaging an area of 5.75 m x 3.20 m. **Fig. 14.c** illustrates substantial damage from the last explosive weight, affecting a substantial portion of the 12 m length and 10 m width of the top slab. Despite this, the connection zone between the cable and the deck maintained a reasonable level of safety.

3.3. Analysis of pylon

Before blast loads were applied, the maximum axial compressive force at the pylon base was $131.66x10^3$ kN. Following the application of three explosive weights, the recorded force values were $133.99x10^3$ kN, $134.16x10^3$ kN, and $135.34x10^3$ kN, respectively (shown in **Fig. 15.a**). The forces at the base displayed closely aligned values, with the largest increase being 2.79%. Notably, due to the substantial distance from the detonation point, the blasting loads indirectly influenced the axial forces by generating excessive tension in the cables, which was then transmitted to the pylon.

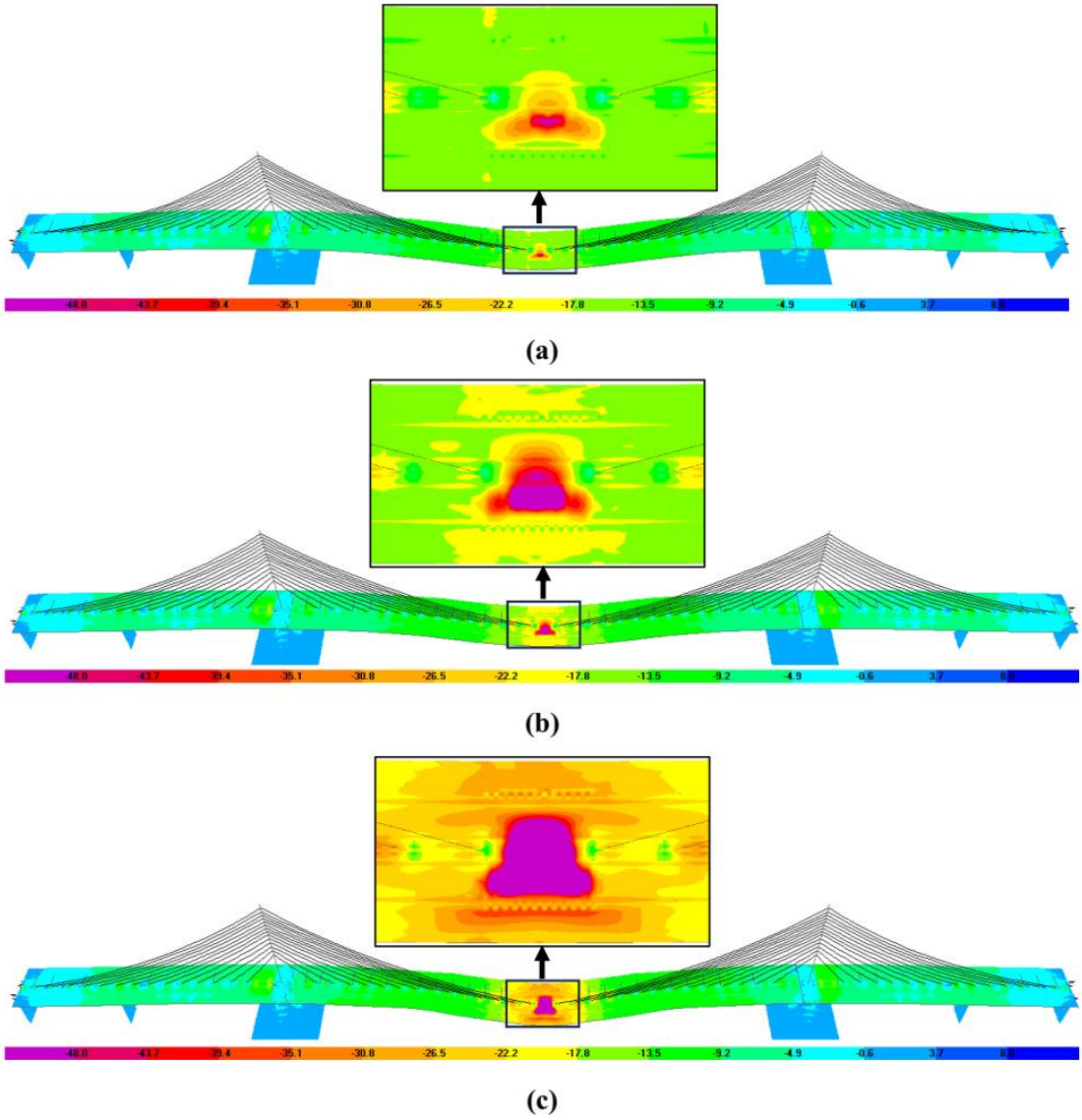

Fig. 14: Stress contour for the top slab along the bridge deck; (Unit: N/mm2); Stresses distribution under 230 kg TNT, (b) Stresses distribution under 680 kg TNT, and (c) Stresses distribution under 2270 kg TNT.

Analyzing shear forces on a pylon is crucial for ensuring structural stability, appropriate material selection, and overall bridge safety. The study revealed significant variations in shear forces between dead loads and live loads, with live loads mitigating the impact on the pylon. Before the explosion, shear forces followed a consistent pattern, ranging from a minimum at

the top to a maximum of 3737 KN at the base. Post-explosion, there was notable fluctuation. Under the first explosive weight, shear force varied, reaching 4638 KN at the base. This trend continued with the second weight, peaking at 4726 KN, indicating a 26.5% increase. For the third weight, the maximum shear force reached 5638 KN, showing a substantial 50.8% increase (**Fig. 15.b**).

Analysing BMs is crucial in the section design process, especially when considering them in conjunction with axial forces. The interplay between BMs and axial forces fundamentally shapes the behaviour of the section, influencing the selection of section properties. **Fig. 15.c** shows the BM of the pylon, showcasing a substantial impact from the explosion. The graph reveals a significant alteration in the response, with a negative BM having the maximum value at the base, reaching 106.96x10^3 kN.m. When applying the first explosive weight, a positive-direction BM at mid-height reached 9.88x10^3 kN.m, while the negative BM at the base slightly increased to 109.65x10^3 kN.m. Using the second explosive weight resulted in a similar pattern, with an increased positive BM of 18.25x10^3 kN.m and a slight rise in the negative BM at the base to 110.77x10^3 kN.m. This demonstrated a double increase in the positive BM when the explosion weight tripled. Utilizing the last weight led to more substantial changes, including a positive BM of 32.46x10^3 kN.m and a slight increase in the negative BM at the base, reaching 111.58x10^3 kN.m.

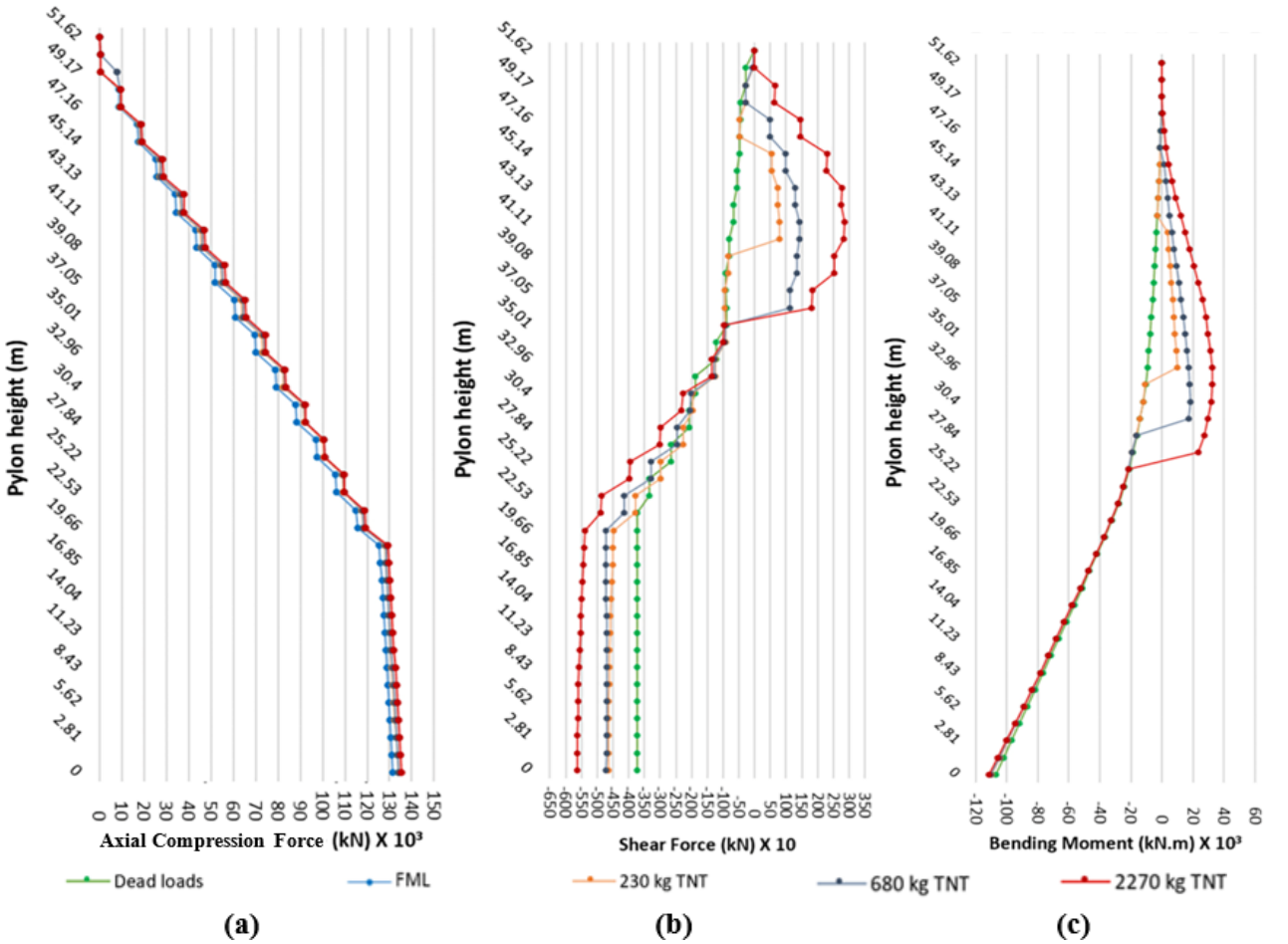

Fig. 15: Straining action diagrams for the single pylon structure; (a) Normal force (Unit: KN), (b) Shear force (Unit: KN), and (c) Bending moment (Unit: kN.m).

4. Conclusions

The study delved into the dynamic response of single-plane prestressed concrete cable-stayed bridges under blast loads, developing a comprehensive shell element model for the Aswan cable-stayed bridge. The investigation included the assessment of the effects of blast weights at 230 kg, 680 kg, and 2270 kg, resulting in the following key findings:

- Regarding cables, consistent with earlier observations, the first five main cables exhibited a noticeable increase in their force values. This pattern was also observed in the corresponding five side cables, albeit with less increase. The variance can be attributed to their passage through a medium, namely the pylon, affirming that the pylon experienced a slight increase in forces.
- The main cables exhibited the most significant rise, peaking at a 19.5% increase in the cable nearest to the detonation point. Meanwhile, the side cables experienced a maximum increase of 6.4%.
- The significant deflection caused by blast loads led to great pressure on the range surrounding the detonation point, resulting in exceeding the maximum stress capacity in some areas of the top slab. The size of damage varied based on the explosive weight.
- Corresponding to the third weight, the affected region in the top slab extended to approximately 12 m in length and 10 m in width.
- Concerning axial forces, the increase was modest, reaching a maximum percentage increase of 2.79% under the third weight compared to the force generated by applying the main loads.
- The pylon's BM experienced significant impact from the explosion, revealing noteworthy alterations in response. The negative BM reached its maximum value at the base, measuring 106.96×10^3 kN.m. Applying different explosive weights resulted in varying positive and negative BMs, with a doubling of the positive BM when the explosion weight tripled. The last weight caused substantial changes, including a positive BM of 32.46×10^3 kN.m and a slight increase in the negative BM at the base, reaching 111.58×10^3 kN.m.

5. Recommendations

- Explore alternative materials or strengthening techniques for the top slab deck to enhance blast resistance.
- Extend analysis to diverse bridge configurations to understand the influence of different designs on blast resistance.
- Develop design guidelines for blast-resistant cable-stayed bridges to assist engineers in improving bridge resilience.

References

[1] Y. Pan, C. E. Ventura, and M. M. S. Cheung, "Performance of highway bridges subjected to blast loads," *Eng Struct*, vol. 151, pp. 788–801, Nov. 2017, Doi: 10.1016/j.engstruct.2017.08.028.

[2] J. Lee, K. Choi, and C. Chung, "Numerical analysis-based blast resistance performance assessment of cable-stayed bridge components subjected to blast loads," *Applied Sciences (Switzerland)*, vol. 10, no. 23, pp. 1–19, Dec. 2020, Doi: 10.3390/app10238511.

[3] R. Mudragada and S. S. Mishra, "Effect of blast loading and resulting progressive failure of a cable-stayed bridge," *SN Appl Sci*, vol. 3, no. 3, Mar. 2021, Doi: 10.1007/s42452-021-04145-y.

[4] S. Trélat, I. Sochet, B. Autrusson, K. Cheval, and O. Loiseau, "Impact of a shock wave on a structure on explosion at altitude," *J Loss Prev Process Ind*, vol. 20, no. 4–6, pp. 509–516, Jul. 2007, Doi: 10.1016/j.jlp.2007.05.004.

[5] S. Trélat, I. Sochet, B. Autrusson, O. Loiseau, and K. Cheval, "Strong explosion near a parallelepipedic structure," *Shock Waves*, vol. 16, no. 4–5, pp. 349–357, May 2007, Doi: 10.1007/s00193-006-0069-3.

[6] J. Lellep and K. Torn, "Shear and bending response of a rigid-plastic beam subjected to impulsive loading," *Int J Impact Eng*, vol. 31, no. 9, pp. 1081–1105, Oct. 2005, Doi: 10.1016/j.ijimpeng.2004.07.008.

[7] S. Peng, L. Jun Cai, T. Hua Jiang, and X. Kai, "Experimental study on blast damage of RC T-beam bridge," *Sensor Review*, vol. 41, no. 4, pp. 397–405, Oct. 2021, Doi: 10.1108/SR-03-2021-0086.

[8] G. Gholipour, C. Zhang, and A. A. Mousavi, "Loading rate effects on the responses of simply supported RC beams subjected to the combination of impact and blast loads," *Eng Struct*, vol. 201, Dec. 2019, Doi: 10.1016/j.engstruct.2019.109837.

[9] G. D. Williams and E. B. Williamson, "Response of Reinforced Concrete Bridge Columns Subjected to Blast Loads," *Journal of Structural Engineering*, vol. 137, no. 9, pp. 903–913, Sep. 2011, Doi: 10.1061/(asce)st.1943-541x.0000440.

[10] S. M. Anas, M. Shariq, M. Alam, A. M. Yosri, A. Mohamed, and M. AbdelMongy, "Influence of Supports on the Low-Velocity Impact Response of Square RC Slab of Standard Concrete and Ultra-High Performance Concrete: FEM-Based Computational Analysis," *Buildings*, vol. 13, no. 5, May 2023, Doi: 10.3390/buildings13051220.

[11] S. M. Anas, M. Alam, and M. Umair, "Experimental and numerical investigations on performance of reinforced concrete slabs under explosive-induced air-blast loading: A state-of-the-art review," *Structures*, vol. 31, pp. 428–461, Jun. 2021, Doi: 10.1016/J.ISTRUC.2021.01.102.

[12] S. K. Hashemi, M. A. Bradford, and H. R. Valipour, "Dynamic response of cable-stayed bridge under blast load," *Eng Struct*, vol. 127, pp. 719–736, Nov. 2016, Doi: 10.1016/j.engstruct.2016.08.038.

[13] S. K. Hashemi, M. A. Bradford, and H. R. Valipour, "Dynamic response and performance of cable-stayed bridges under blast load: Effects of pylon geometry," *Eng Struct*, vol. 137, pp. 50–66, Apr. 2017, Doi: 10.1016/j.engstruct.2017.01.032.

[14] E. K. C. Tang and H. Hao, "Numerical simulation of a cable-stayed bridge response to blast loads, Part I: Model development and response calculations," *Eng Struct*, vol. 32, no. 10, pp. 3180–3192, Oct. 2010, Doi: 10.1016/j.engstruct.2010.06.007.

[15] H. Hao and E. K. C. Tang, "Numerical simulation of a cable-stayed bridge response to blast loads, Part II: Damage prediction and FRP strengthening," *Eng Struct*, vol. 32, no. 10, pp. 3193–3205, Oct. 2010, Doi: 10.1016/j.engstruct.2010.06.006.

[16] C. D. Tetougueni and P. Zampieri, "Structural response of cable-stayed bridge subjected to blast load," in *Procedia Structural Integrity*, Elsevier B.V., 2019, pp. 765–774. Doi: 10.1016/j.prostr.2019.08.225.

[17] J. Son and H. J. Lee, "Performance of cable-stayed bridge pylons subjected to blast loading," *Eng Struct*, vol. 33, no. 4, pp. 1133–1148, Apr. 2011, Doi: 10.1016/j.engstruct.2010.12.031.

[18] W. Zhu, Y. Xiao, J. Yu, J. Jia, and Z. Li, "Damage modes and mechanism of steel-concrete composite bridge slabs under contact explosion," *J Constr Steel Res*, vol. 212, p. 108223, Jan. 2024, Doi: 10.1016/J.JCSR.2023.108223.

[19] J. F. Hassan, A. A. A. Rahman, and D. M. Al-Tarafany, "Prestressed bridge deck responses to blast loads," *IOP Conf Ser Mater Sci Eng*, vol. 1067, no. 1, p. 012003, 2021, Doi: 10.1088/1757-899x/1067/1/012003.

[20] A. Filice, M. Mynarz, and R. Zinno, "Experimental and Empirical Study for Prediction of Blast Loads," *Applied Sciences (Switzerland)*, vol. 12, no. 5, Mar. 2022, Doi: 10.3390/app12052691.

[21] Prof. J. G. C. Suryakant S. Birajdar, "Analysis of Blast Loading on Structural Components," *International Journal of Scientific Engineering and Research (IJSER)*, 2017.

[22] Gilbert F. Kinney and Kenneth J. Graham, *EXPLOSIVE SHOCKS IN AIR*. 1985.

[23] H. L. Brode, "Numerical solutions of spherical blast waves," *J Appl Phys*, vol. 26, no. 6, pp. 766–775, 1955.

[24] N. M., and R. J. Hansen. Newmark, *Design of blast resistant structures*. 1961.

[25] H. L. Brode, "Blast wave from a spherical charge," *Physics of Fluids*, vol. 2, no. 2, pp. 217–229, 1959, Doi: 10.1063/1.1705911.

[26] C. N. Kingery, *Air blast parameters versus distance for hemispherical TNT surface bursts*. 1966.

[27] Vasilis. Karlos, George. Solomos, Bernard. Viaccoz, and European Commission. Joint Research Centre. Institute for the Protection and the Security of the Citizen. *Calculation of blast loads for application to structural components.* Publications Office, 2013.

[28] M. Hasan, E. Khalil, W. Attia, and A. Turkey, "Influence of deck longitudinal prestressing on cable-stayed bridges," *Structural Engineering International*, vol. 25, no. 3, 2015.

[29] J. Yang, J. Wang, S. Zhang, and Z. Wang, "Behavior of eccentrically loaded circular CFRP-steel composite tubed steel-reinforced high-strength concrete columns," *J Constr Steel Res*, vol. 170, 2020, Doi: 10.1016/j.jcsr.2020.106101.

[30] J. B. Mander, M. J. N. Priestley, and R. Park, "Theoretical Stress-Strain Model for Confined Concrete," *Journal of Structural Engineering*, vol. 114, no. 8, pp. 1804–1826, 1988, Doi: 10.1061/(asce)0733-9445(1988)114:8(1804).

[31] A. KAMAL, M. RABEI, A. El-ATTAR, M. KUNIEDA, and H. NAKAMURA, "Ambient Vibration Test of Aswan Cable Stayed Bridge," *J Appl Mech*, vol. 9, 2006, Doi: 10.2208/journalam.9.85.

[32] N. N. Fedorova, S. A. Valger, and A. V. Fedorov, "Simulation of blast action on civil structures using ANSYS Autodyn," *AIP Conf Proc*, vol. 1770, 2016, Doi: 10.1063/1.4963939.

[33] Y. Shi, H. Hao, and Z. X. Li, "Numerical simulation of blast wave interaction with structure columns," *Shock Waves*, vol. 17, no. 1–2, pp. 113–133, 2007, Doi: 10.1007/s00193-007-0099-5.

[34] K. Ali, A. Javed, A. E. Mustafa, and A. Saleem, "Blast-Loading Effects on Structural Redundancy of Long-Span Suspension Bridge Using a Simplified Approach," *Practice*

Periodical on Structural Design and Construction, vol. 27, no. 3, 2022, Doi: 10.1061/(asce)sc.1943-5576.0000699.

[35] Fema and DHS, "Buildings and Infrastructure Protection Series Reference Manual to Mitigate Potential Terrorist Attacks Against Buildings Homeland Security Science and Technology FEMA," 2011.

[36] H. Hao, Y. Hao, J. Li, and W. Chen, "Review of the current practices in blast-resistant analysis and design of concrete structures," *Advances in Structural Engineering*, vol. 19, no. 8. 2016. Doi: 10.1177/1369433216656430.

[37] A. K. M. Anwarul Islam and N. Yazdani, "Performance of AASHTO girder bridges under blast loading," *Eng Struct*, vol. 30, no. 7, 2008, Doi: 10.1016/j.engstruct.2007.12.014.

تأثير أحمال الانفجار على استجابة الكباري الخرسانية سابقة الإجهاد والملجمة بمستوى واحد من الكابلات

الملخص:

على مدار الستين عامًا الماضية، كان هناك العديد من الهجمات الإرهابية التي استهدفت الكباري والبنى التحتية. في حين ركزت معظم الدراسات السابقة على تأثير أحمال الانفجار على الهياكل والمباني التقليدية، هناك أبحاث محدودة حول آثار الانفجارات على الكباري الملجمة بالكابلات. يعد التحقيق في عواقب أحمال الانفجار على الكباري الملجمة بالكابلات مجالًا بالغ الأهمية للدراسة، خاصة فيما يتعلق بحماية البنية التحتية وأمنها. تقدم هذه الدراسة بحثًا تحليليًا شاملاً لتأثير أحمال الانفجار على سلوك الكباري الملجمة بمستوى واحد من الكابلات وذات قطاع صندوقي من الخرسانة سابقة الإجهاد، وتم تطبيق الدراسة على كوبري أسوان الملجم. تضمنت الدراسة ثلاث شحنات من أوزان المتفجرات (متوسطة، عالية، وعالية جداً)، والتي تتوافق مع الحمولة المكافئة للمركبات المتوقع مرورها على الكوبري. تم عمل نموذج متكامل لكافة عناصر الكوبري بطريقة العناصر المحدودة، ساعد هذا النموذج على توفير رؤى دقيقة حول استجابة الكوبري في ظل سيناريوهات الانفجار المختلفة، مع التركيز على العناصر الرئيسية مثل الكابلات والأعمدة وقطاع سطح الكوبري. خلصت الدراسة الى أن التشوهات الناتجة عن الانفجار أدت إلى تلف بعض الأجزاء في البلاطة العلوية مسبقة الإجهاد، حيث تختلف مساحة التلف باختلاف الوزن المستخدم. تسبب الوزن الأكبر في أضرار جسيمة؛ بلغت فيها مساحة التلف ١٢م طولاً و ١٠م عرضاً. وواجهت الكابلات القريبة من نقطة التفجير زيادة في قوى الشد، حيث بلغت أكبر نسبة زيادة في قوى الشد ١٩٪. اما بالنسبة للأبراج، فلقد زادت القوى المحورية بشكل بسيط، وكان لتوزيع عزوم الإنحناء تغييرات ملحوظة تحت تأثير الأوزان المختلفة. حيث تم تسجيل أكبر قيمة عزم إنحناء عند القاعدة تحت تأثير الأحمال الميتة، بينما زادت قيم عزم الإنحناء عند منتصف الارتفاع تحت تأثير شحنات الانفجار المختلفة، مع عدم وجود تغيير ملحوظ في القيم عند القاعدة.

تعد دراسة تأثير أحمال الانفجار على الكباري الملجمة بالكابلات أمرًا حيويًا لتعزيز مرونتها وسلامتها ضد التهديدات الأمنية أو الحوادث المختلفة. يقدم هذا البحث معلومات لتحسين التصميم وتدابير السلامة واستراتيجيات تخفيف المخاطر الفعالة، مما يساهم في تعزيز المقاومة الشاملة للانفجارات والموثوقية طويلة المدى لهذه الهياكل الحيوية والفريدة.